P H Y S I C A L   R E V I E W   L E T T E R S

Femtosecond Undulator Radiation from Sliced Electron Bunches

S. Khan,[1,*] K. Holldack,[1] T. Kachel,[1] R. Mitzner,[2] and T. Quast[1]

[1]*Berliner Elektronenspeicherring-Gesellschaft für Synchrotronstrahlung m.b.H. (BESSY),*
Albert-Einstein-Straße 15, 12489 Berlin, Germany
[2]*Physikalisches Institut der Universität Münster, Wilhelm-Klemm-Straße 10, 48149 Münster, Germany*

At the 1.7-GeV electron storage ring BESSY II, a first source of synchrotron radiation with 100 fs pulse duration, variable (linear and circular) polarization, tunable photon energy (300 to 1400 eV), and excellent signal-to-background ratio was constructed and is now in routine operation.

PACS numbers: 41.60.Ap, 41.75.Ht, 42.65.Re

At contemporary synchrotron radiation (SR) sources, powerful x-ray techniques to study the structure and function of matter are limited in time resolution by the electron bunch length of 30–100 ps [full width at half-maximum (FWHM)], whereas the 100-fs time scale, on which chemical reactions or phase transitions take place, has been accessible in the visible regime by lasers since the mid-1980s [1]. In the quest for short pulse duration *and* short wavelength, one route is to convert femtosecond (fs) laser pulses to x rays by higher-harmonic generation [2] (where the flux drops rapidly with increasing photon energy) or by a laser-produced plasma [3] (emitting fully divergent x rays and lacking tunability). Another possibility is to manipulate the time structure of relativistic electron bunches to produce shorter SR pulses. With ultrashort and intense x-ray pulses from Å-wavelength free-electron lasers (FELs) still in the future [4,5], techniques have been devised to improve the time resolution of present-day SR sources by 2 [6,7] or even 3 orders of magnitude [8]. The latter approach, ''slicing'' electron bunches by fs laser pulses, was experimentally demonstrated [9] and applied to x-ray absorption spectroscopy [10] at the Advanced Light Source in Berkeley with radiation from a bend magnet. A first facility to produce 100-fs undulator radiation with linear and circular polarization and photon energies up to 1400 eV was constructed in 2004 at the 1.7-GeV electron storage ring BESSY II in Berlin and is now in routine operation for pump-probe experiments. Compared to a bend magnet source, an undulator not only increases the photon flux per bandwidth by orders of magnitude, but allows one to extract the ultrashort radiation component with extremely low background, as explained below and demonstrated by the results presented in this Letter.

The principle and technical layout of the novel fs x-ray source is illustrated by Fig. 1. Pulses from a Ti:sapphire laser system (wavelength $\lambda_L = 780$ nm, pulse duration 30–50 fs (FWHM), pulse energy ≤ 2.8 mJ at 1 kHz repetition rate [11]) copropagate with electron bunches in a planar undulator (U139, the ''modulator'' with period length $\lambda_U = 139$ mm and $N_U = 10$ periods). In the laser-electron overlap region, an oscillatory modulation $\delta E(z)/E$ of the

electron energy E along the longitudinal coordinate z with a periodicity of λ_L and an amplitude reaching $|\delta E/E|_{\max} \equiv \Delta E/E \sim 1\%$ is obtained, provided the resonance condition

$$\lambda_L = \frac{\lambda_U}{2\gamma^2}\left(1 + \frac{K^2}{2}\right) \qquad (1)$$

is fulfilled, where γ is the Lorentz factor of the electrons and K is the undulator deflection parameter. Energy-
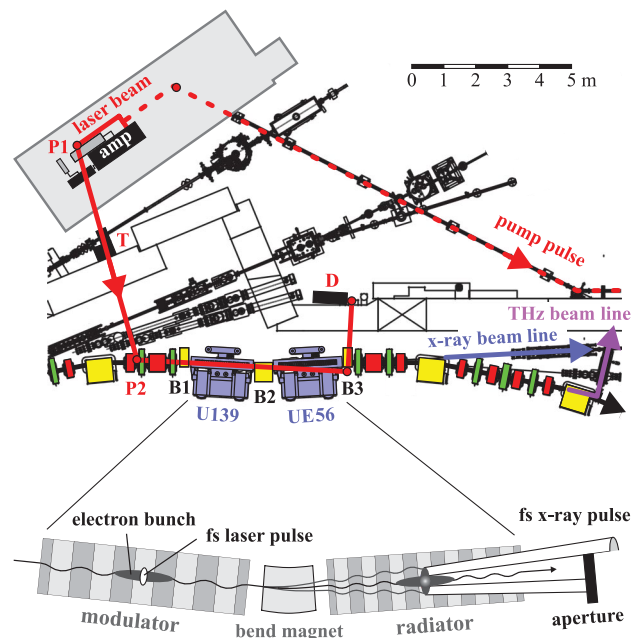

FIG. 1 (color). BESSY II floor plan (top) and schematic view (bottom) of modulator (U139), radiator (UE56), and a bend magnet (B2) for angular short-pulse separation. Also shown are the storage ring dipole (yellow), quadrupole (red), and sextupole magnets (green). Pulses from a Ti:sapphire amplifier (amp) pass two periscopes (P1, P2) and a telescope (T) before interacting with the electron beam, while a 10% fraction is sent as pump pulses (dashed red line) to the experiment at the x-ray beam line (blue). Diagnostics (D) provides timing signals and images of laser and U139 radiation. The interaction efficiency is monitored by coherent THz radiation (magenta).

modulated electrons are displaced horizontally by a subsequent dipole magnet (B2, bend angle 112 mrad) in order to extract their radiation—the fs x-ray pulse—from a second undulator (UE56, the ''radiator,'' an elliptical undulator with 30 periods of 56 mm length). Picosecond (ps) radiation from the main bunch is blocked below a certain angle relative to the electron beam axis. Depending on this cutoff angle, the resulting short-pulse intensity is about 10^{-4} of the total bunch radiation and the residual ps background is 10–100 times lower. By steering the electron beam away from the UE56 axis, radiation from electrons with $\delta E/E < 0$ is aligned with the x-ray beam line, while the bulk of radiation from the UE56 and adjacent bend magnets (B2, B3) is not. Even though the small vertical emittance in a storage ring suggests vertical separation by focusing the radiation on an aperture, as described in [9], a horizontal angular separation scheme (also proposed in [9]) was employed at BESSY to avoid nonspecular scattering from focusing mirrors, which may cause excessive background. Another advantage of this scheme is that non-Gaussian tails of the electron beam (another potential background source) are negligible due to the large radiation divergence. It should, however, be noted that angular separation is feasible only for an undulator as radiator, since (i) the angular distribution of bend magnet or wiggler radiation is much wider, particularly in the deflecting (usually horizontal) plane, and (ii) vertical angular separation would be inacceptable in a storage ring because of the required large bend angle.

In April 2004, the undulators (U139, UE56) and three bend magnets (B1, B2, B3 in Fig. 1) were installed and the UE56 x-ray beam lines were substantially modified. After an extensive commissioning period, the spatial and temporal laser-electron overlap is now established within minutes and maintained indefinitely. As discussed in detail elsewhere [12], path length differences of energy-modulated electrons create a subpicosecond dip with side lobes in the longitudinal bunch profile, which gives rise to intense coherent THz radiation. Using a dedicated THz beam line at a bend magnet 11 m downstream of the modulator, the laser-electron overlap is optimized by a feedback loop controlling two laser mirrors and adjusting the laser timing.

The energy-modulation process was studied by directly probing the electron energy distribution, moving a scraper horizontally towards the electron beam while measuring changes of the beam current with a Si photodiode [13]. The observed electron loss rate is proportional to the number of electrons with a modulation amplitude of

$$\Delta E/E \geq \frac{\Delta x}{\sqrt{\beta_S}\sqrt{\gamma D^2 + 2\alpha DD' + \beta D'^2}}. \quad (2)$$

Here, β, α, γ, D, and D' are the optical functions (Twiss parameters, dispersion, and its derivative [14]) at the modulator and β_S is the beta function at the scraper, where

the dispersion is zero. Measurements with laser pulse energies E_L from 1.2 to 2.15 mJ are compared in Fig. 2 with respective simulations [15], obtaining energy-modulation amplitudes which are compatible with the predicted [8] trend $\Delta E/E \sim \sqrt{E_L}$ (see inset, solid line). However, the pulse energies used in the simulation to reproduce the data (also shown in the inset) are $\sim 1/2$ of the measured ratio of laser power and repetition rate. Despite this discrepancy (similarly reported in [9]), which can be explained by optical aberrations and a nonoptimal laser beam size, sufficient energy modulation to generate fs x-ray pulses is routinely obtained.

The x-ray pulse duration depends on the laser pulse length, the slippage of the electrons with respect to the laser field ($N_U\lambda_L/c = 26$ fs), and electron path length differences between modulator and radiator:

$$\Delta l = R_{51}x + R_{52}x' + R_{56}\delta E/E, \quad (3)$$

where x and x' are the horizontal phase space coordinates at the entrance of bend magnet B2 and the coefficients R_{ij} are given by its bend angle and length [14]. In the UE56 plane-grating monochromator beam line [16], x-ray pulse lengthening (~ 30 fs) is given by the number of illuminated grating lines times the wavelength. For typical settings, simulations of the laser-electron interaction combined with electron tracking calculations yield an overall pulse duration of 100 fs (FWHM), dominated by the first term of Eq. (3). The same calculations predict a 300-fs dip in the longitudinal bunch profile at the THz beam line, which is consistent with measured far-infrared spectra [12]. In addition, recent pump-probe experiments (to be published) suggest a time resolution of 150 fs, including optical path variations over a period of 8 h.

The generated fs photon flux per 0.1% bandwidth is of the order of 10^3 per laser pulse (or 10^6 per s) and can be
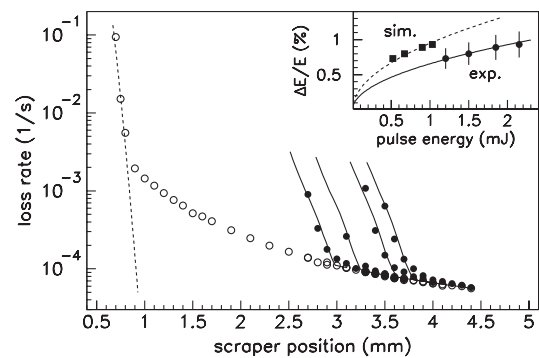

FIG. 2. Electron loss rate versus scraper position with (black dots) and without (open symbols) laser-induced energy modulation under variation of the laser pulse energy. The solid lines are simulation results and the dashed line represents the quantum lifetime limit, from which the beam position was deduced. Inset: modulation amplitude $\Delta E/E$ as function of the actually applied (dots) and simulated (squares) pulse energy. Error bars reflect the uncertainty in the optical functions.

inferred by comparing measured angular photon distributions with SR simulations. The photon flux on the sample under study is typically 2 orders of magnitude lower, given by the beam line transmission and depending on photon energy and monochromator settings. This was verified by single-photon detection with an avalanche photodiode (APD), cross calibrated with the photocurrent of a GaAs diode. The rate of actually detected photons, deduced from the APD count rate and average pulse height and limited by the energy-dependent detector efficiency ($\sim 20\%$ at 700 eV), is of the order 10^3 per s and 0.1% bandwidth.

Detected photon rates under variation of the cutoff angle for linear (vertical) polarization and photon energies from 400 to 1200 eV with and without laser-induced energy modulation are shown in Fig. 3, demonstrating the excellent signal-to-background ratio at, e.g., the M edges of rare-earth elements, the L edges of Ni and Fe, down to the K edges of O and N. Among these cases, short-pulse separation is most difficult for 530 eV, since the angular distribution of the UE56 third harmonic broadens with increasing deflection parameter K (i.e., smaller photon energy), whereas 400 eV is reached by the first harmonic and smaller K. The cutoff angle can be used to trade photon flux against signal-to-background ratio.

If the laser interacts with only one electron bunch at a rate of 1 kHz, the signal-to-background ratio is reduced (Fig. 3, dashed lines) by additional ps background due to off-energy electrons from previous laser shots (open symbols). Energy modulation in a dispersive region excites a synchrotron oscillation as well as horizontal betatron motion, and the temporal evolution of the resulting radiation was studied. As shown in Fig. 4, there is a modulation of 14 kHz (twice the synchrotron frequency) from the synchrotron motion of electrons with opposite $\delta E/E$, decaying with a time constant of 1.6 ms and merging in a smooth background of 5 ms decay time (see inset). On top of that, there is a 200-kHz modulation, corresponding to the aliased betatron frequency $f_\circ(1 - q)$, where $f_\circ = 1.25$ MHz is the revolution frequency and $q = 0.84$ is the fractional tune. Although the radiation damping time is 10 ms, this modulation decays with a time constant of 0.1 ms (2200 betatron cycles), because (i) the betatron phase randomizes, and (ii) it takes less than the damping time to reduce the radiation angle below the cutoff angle. To maximize the fs x-ray flux, the background after 1 ms is tolerated and the laser interacts with a single bunch of enhanced current (5–10 mA) added to a 250 mA multi-bunch pattern. Upgrading to higher rates, however, would necessitate a more complex bunch pattern such that the laser interacts with several bunches in turn [18].

For circular polarization, which is a key feature of the BESSY fs x-ray source, radiation of opposite helicity within the fs pulse must be considered. Calculations [19] for the UE56 tuned to the third harmonic at 850 eV with near-circular polarization show that the angular photon
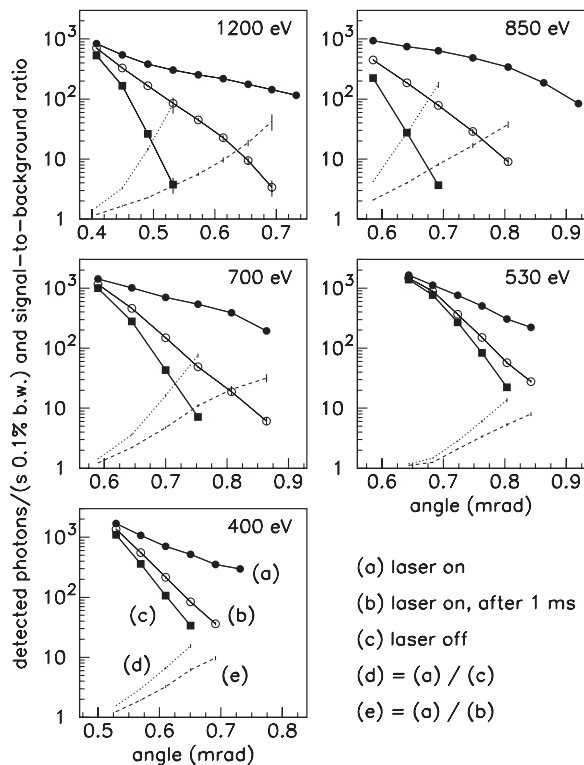

FIG. 3. Detected photon rate per 0.1% bandwidth (normalized to a bunch current of 7 mA) versus cutoff angle for linearly polarized photons from 400 to 1200 eV with (a) and without (c) laser-induced energy modulation as well as 1 ms after the laser pulse (b). Also shown are the respective signal-to-background ratios (d) = (a)/(c) and (e) = (a)/(b).
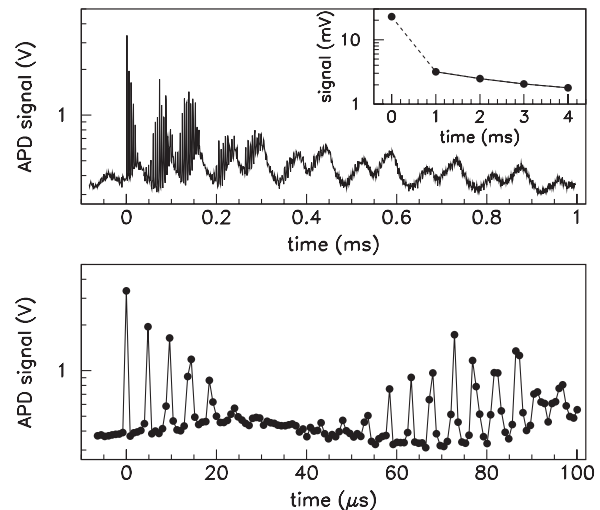

FIG. 4. Signal from photons at 850 eV (linear polarization, cutoff angle 0.69 mrad) as function of time after laser-electron interaction, exhibiting a 200-kHz modulation from betatron oscillations (bottom, one data point per turn), a 14-kHz modulation from synchrotron oscillations (top), and a residual background with a decay time of 5 ms (inset), measured earlier with a laser repetition rate of 200 Hz [17].
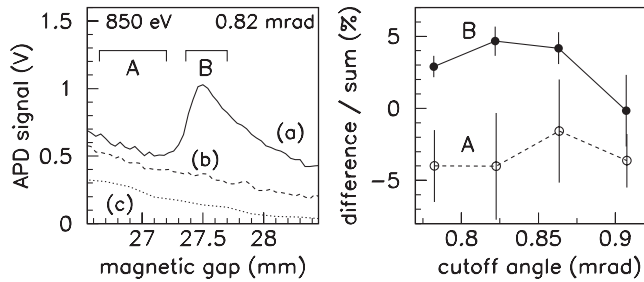
FIG. 5. Signals from circularly polarized photons at 850 eV versus UE56 magnetic gap (left) with (a) and without (c) laser-induced energy modulation, and 1 ms after the laser pulse (b). The fs radiation component is (a) − (b). The difference of fs radiation (normalized to its sum) transmitted by a Ni sample for opposite magnetization is shown as a function of cutoff angle (right) for the indicated gap regions (A, B).

distribution is divided into two regions. Photons emitted at angles below 0.2 mrad between the electron and photon direction exhibit a resonant energy spectrum (that of the third harmonic) and have the intended helicity. Photons emitted at larger angles show a flat energy distribution, since they can be viewed as redshifted tails of higher harmonics, and have the opposite helicity. In this particular case and not necessarily true for other undulator settings, a flat component in the photon spectrum is indicative of helicity-diluting background. This is shown in Fig. 5, where spectra were recorded by setting the monochromator to 850 eV while scanning the UE56 magnetic gap. As before, the measured signal (a) comprises ps background (b) and fs radiation (a)–(b), their ratio depending on the cutoff angle. The helicity of fs radiation was probed at the third harmonic (B) and at smaller gap (A) using x-ray magnetic circular dichroism, i.e., the difference in x-ray absorption, here at the L_3 edge of Ni, for magnetization parallel or antiparallel to the helicity vector. This difference, normalized to the sum of fs radiation (Fig. 5, right) changes sign—i.e., the helicity reverses—when the magnetic gap is tuned from region A to B. The degree of circular polarization on the harmonic can be maximized by variation of the cutoff angle, as shown in Fig. 5, but also by optimizing the energy-modulation amplitude and by limiting the photon distribution with a vertical aperture.

The rate of detected fs photons may be increased by up to 3 orders of magnitude by upgrading the laser to a higher repetition rate (factor 3–5), by using a beam line with better transmission (under construction, factor 8–10), by larger detection efficiency (factor 2–4), and by using multiple detectors to measure photons at different energies simultaneously (factor 5–10). Finally, the novel fs x-ray source provides a unique opportunity to gain hands-on experience for future FELs in view of laser-based seeding schemes, e.g., [20], attosecond-pulse generation [21,22], short-pulse diagnostics, and synchronization techniques.

*Now at Universität Hamburg, Institut für Experimentalphysik, Luruper Chaussee 149, 22761 Hamburg, Germany.
Electronic address: shaukat.khan@desy.de

[1] D. Strickland and G. Mourou, Opt. Commun. **55**, 447 (1985).
[2] E. Seres, J. Seres, F. Krausz, and C. Spielmann, Phys. Rev. Lett. **92**, 163002 (2004).
[3] C. Rischel et al., Nature (London) **390**, 490 (1997).
[4] J. Arthur et al., LCLS Conceptual Design Report No. SLAC-R-593, 2002.
[5] TESLA XFEL Technical Design Report Supplement, edited by R. Brinkmann et al., Report No. DESY 2002-167, 2002.
[6] M. Abo-Bakr et al., Phys. Rev. Lett. **90**, 094801 (2003).
[7] A. Zholents, P. Heimann, M. Zolotorev, and J. Byrd, Nucl. Instrum. Methods Phys. Res., Sect. A **425**, 385 (1999).
[8] A. A. Zholents and M. S. Zolotorev, Phys. Rev. Lett. **76**, 912 (1996).
[9] R. W. Schoenlein et al., Appl. Phys. B **71**, 1 (2000); Science **287**, 2237 (2000).
[10] A. Cavalleri et al., Phys. Rev. Lett. **95**, 067405 (2005).
[11] Kapteyn-Murnane Laboratories MTS oscillator and HAP-AMP amplifier; Coherent Verdi V5; Quantronix 527DQE-S.
[12] K. Holldack, S. Khan, R. Mitzner, and T. Quast, Phys. Rev. Lett. **96**, 054801 (2006).
[13] R. Thornagel, R. Klein, and G. Ulm, Metrologia **38**, 385 (2001).
[14] K. Brown, in Handbook of Accelerator Physics and Engineering, edited by A. W. Chao and M. Tigner (World Scientific, Singapore, 1999).
[15] K. Holldack, T. Kachel, S. Khan, R. Mitzner, and T. Quast, Phys. Rev. ST Accel. Beams **8**, 040704 (2005).
[16] M. R. Weiss et al., Nucl. Instrum. Methods Phys. Res., Sect. A **467**, 449 (2001).
[17] S. Khan, K. Holldack, R. Mitzner, and T. Quast, in Proceedings of the Particle Accelerator Conference, Knoxville, 2005, www.jacow.org, p. 2309.
[18] S. Khan, in Proceedings of the Particle Accelerator Conference, Knoxville, 2005, www.jacow.org, p. 2327.
[19] W. Frentrup (private communication).
[20] L. H. Yu, Phys. Rev. A **44**, 5178 (1991).
[21] E. L. Saldin, E. A. Schneidmiller, and M. V. Yurkov, Opt. Commun. **239**, 161 (2004).
[22] A. A. Zholents and W. M. Fawley, Phys. Rev. Lett. **92**, 224801 (2004).